Available online at www.sciencedirect.com
ScienceDirect
Comput. Methods Appl. Mech. Engrg. 296 (2015) 18–38
Computer methods in applied mechanics and engineering
www.elsevier.com/locate/cma

The harmonic balance method for bifurcation analysis of large-scale nonlinear mechanical systems

T. Detroux*, L. Renson, L. Masset, G. Kerschen

Space Structures and Systems Laboratory, Department of Aerospace and Mechanical Engineering, University of Liège, Liège, Belgium

Received 3 April 2015; received in revised form 14 July 2015; accepted 16 July 2015
Available online 23 July 2015

Abstract

The harmonic balance (HB) method is widely used in the literature for analyzing the periodic solutions of nonlinear mechanical systems. The objective of this paper is to exploit the method for bifurcation analysis, i.e., for the detection and tracking of bifurcations of nonlinear systems. To this end, an algorithm that combines the computation of the Floquet exponents with bordering techniques is developed. A new procedure for the tracking of Neimark–Sacker bifurcations that exploits the properties of eigenvalue derivatives is also proposed. The HB method is demonstrated using numerical experiments of a spacecraft structure that possesses a nonlinear vibration isolation device.

Keywords: Harmonic balance; Continuation of periodic solutions; Bifurcation detection and tracking; Floquet exponents; Quasiperiodic oscillations; Detached resonance curves

1. Introduction

Nonlinear systems are known to exhibit rich and complex dynamical behaviors, which linear systems cannot. These behaviors include, for instance, modal interactions, detached resonance curves, quasiperiodic oscillations, bifurcations and chaos. Even though periodic solutions represent only a subset of the dynamical attractors of nonlinear systems, their computation and interpretation usually provide great insight into the system's dynamics. Different algorithms and numerical methods for the computation of periodic solutions can be found in the literature. Most of them build on a continuation procedure [1], as a means of studying the evolution of the periodic solutions with respect to the frequency of the harmonic forcing or a design parameter.

Time-domain methods, which deal with the resolution of a boundary value problem (BVP), have proven effective for low-dimensional problems. When applied to larger systems, their computational burden can become substantial. For example, the shooting technique requires numerous time integrations that can slow down the algorithm. Efforts

* Correspondence to: Space Structures and Systems Laboratory, Department of Aerospace and Mechanical Engineering, University of Liège, 1 Chemin des Chevreuils (B52/3), B-4000 Liège, Belgium.
E-mail addresses: tdetroux@ulg.ac.be (T. Detroux), l.renson@ulg.ac.be (L. Renson), luc.masset@ulg.ac.be (L. Masset), g.kerschen@ulg.ac.be (G. Kerschen).

http://dx.doi.org/10.1016/j.cma.2015.07.017
0045-7825/

have been undertaken to make shooting less computationally intensive by using parallelization [2] and sensitivity analysis [3]. Methods based on orthogonal collocation are utilized in several software for bifurcation detection and tracking, e.g., AUTO [4], COLSYS [5], CONTENT [6], MATCONT [7], and, more recently, COCO [8]. In spite of its high accuracy and ability to address stiff problems, orthogonal collocation is rarely employed for large systems, which can be explained by the considerable memory space required for the discretization of the BVP.

Among all methods in the frequency domain, harmonic balance (HB) is certainly the most widely used method. It is also known as the Fourier–Galerkin method, since it consists in the application of the Galerkin method with Fourier basis and test functions. The periodic signals are approximated with their Fourier coefficients, which become the new unknowns of the problem. The term 'harmonic balance' was first introduced by Krylov and Bogoliubov [9] who performed linearization of nonlinear dynamical equations with single-harmonic approximations. In the 1960s a demonstration of the convergence of the method for Fourier approximations truncated to several harmonics was offered by Urabe [10]. The main advantage of HB is when low orders of approximation are sufficient to obtain an accurate solution, which usually holds for smooth nonlinearities. In this case, the method involves algebraic equations with less unknowns than for orthogonal collocation. The reader can refer to [11] for a comparison between HB and orthogonal collocation applied to smooth and nonsmooth nonlinearities.

Several improvements and adaptations to the HB method were brought in the literature during the last couple of decades. The incremental HB applies the incremental procedure to the equations of motion before the harmonic approximation and balance (see [12,13] or, more recently, [14]). Taking advantage of the fast Fourier transform, Cameron et al. proposed the alternating frequency–time domain (AFT) method that evaluates the nonlinear terms of the equations in the time domain where their analytical expression is known [15]. Since then, many studies utilized the AFT method [16–18]. Similar developments led to the hybrid frequency–time domain method, with applications to systems with dry friction [19,20]. HB was also coupled with continuation schemes, e.g., with arc-length continuation [21] or the so-called asymptotic numerical method [22,23] in the MANLAB package. In [24], a new adaptive HB method was proposed for which the number of harmonics for each degree of freedom (DOF) is automatically selected during the continuation process.

HB has enjoyed numerous applications in the literature. In electrical engineering, Kundert et al. reported its superiority over time-domain techniques for the simulation of nonlinear circuits [25]. Using a well-known variant of the method based on single-harmonic approximations, the so-called describing function (DF) method, Genesio et al. [26] provided analytical expressions for regions of chaotic behavior of Lur'e systems. Other studies were carried out, e.g., for piezoelectric inertial generators [27] or DC–DC converters [28].

Following a pioneer work on wing-control surface flutter [29], the HB method was successfully applied to aeroelastic systems, e.g., to airfoils with freeplay [30] and cubic stiffness [31]. A comparative review of HB applied to limit cycle oscillations can be found in [32]. More recently, fluid dynamics problems where unsteady flows are periodic in time were also tackled. In [33], Hall et al. formulated the HB method for the Navier–Stokes equations, and applications can be found for flows in multi-stage turbomachinery [34,35] and helicopter blades [36].

In mechanical engineering, Cardona et al. developed a multi-harmonic resolution scheme for vibration analysis with nonsmooth nonlinear functions [37]. The HB method was then applied to realistic examples including bladed disks [38], bolted joints [18,39], rotor/stator contacts [21], vibro-impact systems [40,41], geometrically nonlinear beams [42] and plates [43]. The dynamics of complete vehicles [44] and full-scale aircraft [45] were also examined with HB, which demonstrates its effectiveness when applied to reduced finite element models. Comparisons between experiments and the results of HB simulations gave further evidence of the accuracy of the method [46,47].

Beyond applications to classical vibration problems, HB was exploited for extending linear modal analysis to nonlinear systems [48]. Specifically, thanks to its natural filtering property, the computation of nonlinear normal modes (NNMs) and their interactions could be substantially improved [49,50]. As a result, HB formed the basis of a NNM-based model updating strategy and of convergence studies for nonlinear reduced order models [51]. Nonlinear Fourier-based modal analysis was adapted to non-conservative autonomous dynamical systems in [52] thanks to generalized Fourier series with slow and fast time scales. Through this approach, refined later in [53], NNMs of damped systems could be constructed and were found to give an accurate approximation of nonlinear resonances. By extending the spectral basis to two incommensurate frequencies, quasiperiodic (QP) oscillations can be studied, e.g., for monoharmonic [54,55] and bi-periodic excitations [56,57]. Another interesting feature of nonlinear systems, namely the presence of co-existing periodic solutions and detached resonance curves, was studied in [58] by coupling HB with Groebner bases.

The stability of nonlinear solutions can be studied by embedding Floquet theory within the HB formalism [21], which is referred to as Hill's method [59]. In [60], Lanza et al. provided an analytical approximation of Floquet exponents using the DF method. A semi-analytical version was developed by Bonani and Gilli for an arbitrary number of harmonics [61]. However, these developments are limited to systems expressed in Lur'e form. Recently, more general theories have been proposed to compute Floquet exponents for autonomous [62] and nonautonomous [63,64] systems.

Beside stability, bifurcations play a key role in the analysis of nonlinear systems. For example, fold bifurcations translate into a stability change of the periodic solutions, whereas QP oscillations are created or eliminated through Neimark–Sacker (NS) bifurcations. However, even if there exists a large body of literature on HB applied to nonlinear systems, very few studies attempted to use the method for tracking bifurcations. In [60], bifurcation tracking is limited to single-harmonic approximations. Piccardi [65] proposed a procedure to obtain flip and fold curves (and even conditions for codimension-2 bifurcations [66]), but this procedure cannot describe NS bifurcations. Traversa et al. developed a bifurcation tracking technique adapted to fold, flip and NS bifurcations [62] by appending to the HB equation system an equation which describes the considered bifurcations through the Floquet multipliers. However, the resolution of the extra equation with the secant method makes the implementation inefficient when the size of the system increases.

In this context, the main contribution of the present paper is to adapt classical tools for bifurcation analysis in codimension-2 parameter space to the HB formalism. Because we target large-scale mechanical systems with localized nonlinearities, an algorithm that efficiently combines the computation of the Floquet exponents and bordering techniques is developed. A new procedure for the tracking of NS bifurcations that exploits the properties of eigenvalue derivatives is also proposed.

The paper is organized as follows. Section 2 recalls the theory of HB and its formulation in the framework of a continuation algorithm. In Section 3, Hill's method is introduced for assessing the stability of periodic solutions and for detecting their bifurcations. The proposed bifurcation tracking procedure is then presented with its adaptations for fold, branch point and NS bifurcations. The overall methodology is demonstrated using numerical experiments of a spacecraft structure that possesses a nonlinear vibration isolation device. Finally, the conclusions of the present study are summarized in Section 5.

2. Harmonic balance for periodic solutions

2.1. Formulation of the dynamics in the frequency domain

We consider nonautonomous nonlinear dynamical systems with n DOFs governed by the equations of motion

$$\mathbf{M}\ddot{\mathbf{x}} + \mathbf{C}\dot{\mathbf{x}} + \mathbf{K}\mathbf{x} + \mathbf{f}_{nl}(\mathbf{x}, \dot{\mathbf{x}}) = \mathbf{f}_{ext}(\omega, t) \tag{1}$$

where $\mathbf{M}$, $\mathbf{C}$ and $\mathbf{K}$ are the mass, damping and stiffness matrices, respectively. Vectors $\mathbf{x}$, $\mathbf{f}_{nl}$ and $\mathbf{f}_{ext}$ represent the displacements, the nonlinear forces and the periodic external forces that are considered to be harmonic with frequency ω herein. The dots refer to the derivatives with respect to time t.

The periodic signals $\mathbf{x}(t)$ and $\mathbf{f}(\mathbf{x}, \dot{\mathbf{x}}, \omega, t) = \mathbf{f}_{ext}(\omega, t) - \mathbf{f}_{nl}(\mathbf{x}, \dot{\mathbf{x}})$ in Eq. (1) are approximated by Fourier series truncated to the N_Hth harmonic:

$$\mathbf{x}(t) = \frac{\mathbf{c}_0^x}{\sqrt{2}} + \sum_{k=1}^{N_H} \left(\mathbf{s}_k^x \sin\left(\frac{k\omega t}{\nu}\right) + \mathbf{c}_k^x \cos\left(\frac{k\omega t}{\nu}\right) \right) \tag{2}$$

$$\mathbf{f}(t) = \frac{\mathbf{c}_0^f}{\sqrt{2}} + \sum_{k=1}^{N_H} \left(\mathbf{s}_k^f \sin\left(\frac{k\omega t}{\nu}\right) + \mathbf{c}_k^f \cos\left(\frac{k\omega t}{\nu}\right) \right) \tag{3}$$

where $\mathbf{s}_k$ and $\mathbf{c}_k$ represent the vectors of the Fourier coefficients related to the sine and cosine terms, respectively, and the integer ν accounts for subharmonics of the excitation frequency ω. The Fourier coefficients of $\mathbf{f}(t)$, $\mathbf{c}_k^f$ and $\mathbf{s}_k^f$, depend on the Fourier coefficients of the displacements $\mathbf{x}(t)$, $\mathbf{c}_k^x$ and $\mathbf{s}_k^x$, which represent the new unknowns of the

problem. These coefficients are gathered into the $(2N_H + 1)\, n \times 1$ vectors

$$\mathbf{z} = \left[\left(\mathbf{c}_0^x\right)^T \quad \left(\mathbf{s}_1^x\right)^T \quad \left(\mathbf{c}_1^x\right)^T \quad \dots \quad \left(\mathbf{s}_{N_H}^x\right)^T \quad \left(\mathbf{c}_{N_H}^x\right)^T \right]^T \tag{4}$$

$$\mathbf{b} = \left[\left(\mathbf{c}_0^f\right)^T \quad \left(\mathbf{s}_1^f\right)^T \quad \left(\mathbf{c}_1^f\right)^T \quad \dots \quad \left(\mathbf{s}_{N_H}^f\right)^T \quad \left(\mathbf{c}_{N_H}^f\right)^T \right]^T. \tag{5}$$

The displacements and forces are recast into a more compact form

$$\mathbf{x}(t) = (\mathbf{Q}(t) \otimes \mathbb{I}_n)\, \mathbf{z} \tag{6}$$

$$\mathbf{f}(t) = (\mathbf{Q}(t) \otimes \mathbb{I}_n)\, \mathbf{b} \tag{7}$$

where $\otimes$ and $\mathbb{I}_n$ stand for the Kronecker tensor product and the identity matrix of size n, respectively, and $\mathbf{Q}(t)$ is a vector containing the sine and cosine series

$$\mathbf{Q}(t) = \left[\frac{1}{\sqrt{2}} \quad \sin\left(\frac{\omega t}{\nu}\right) \quad \cos\left(\frac{\omega t}{\nu}\right) \quad \dots \quad \sin\left(N_H \frac{\omega t}{\nu}\right) \quad \cos\left(N_H \frac{\omega t}{\nu}\right) \right]. \tag{8}$$

Velocities and accelerations can also be defined using the Fourier series [18], with

$$\dot{\mathbf{x}}(t) = \left(\dot{\mathbf{Q}}(t) \otimes \mathbb{I}_n\right) \mathbf{z} = \left((\mathbf{Q}(t)\boldsymbol{\nabla}) \otimes \mathbb{I}_n\right) \mathbf{z} \tag{9}$$

$$\ddot{\mathbf{x}}(t) = \left(\ddot{\mathbf{Q}}(t) \otimes \mathbb{I}_n\right) \mathbf{z} = \left(\left(\mathbf{Q}(t)\boldsymbol{\nabla}^2\right) \otimes \mathbb{I}_n\right) \mathbf{z} \tag{10}$$

where

$$\boldsymbol{\nabla} = \begin{bmatrix} 0 & & & & \\ & \ddots & & & \\ & & \boldsymbol{\nabla}_k & & \\ & & & \ddots & \\ & & & & \boldsymbol{\nabla}_{N_H} \end{bmatrix}, \qquad \boldsymbol{\nabla}\boldsymbol{\nabla} = \boldsymbol{\nabla}^2 = \begin{bmatrix} 0 & & & & \\ & \ddots & & & \\ & & \boldsymbol{\nabla}_k^2 & & \\ & & & \ddots & \\ & & & & \boldsymbol{\nabla}_{N_H}^2 \end{bmatrix} \tag{11}$$

with

$$\boldsymbol{\nabla}_k = \begin{bmatrix} 0 & -\dfrac{k\omega}{\nu} \\ \dfrac{k\omega}{\nu} & 0 \end{bmatrix}, \qquad \boldsymbol{\nabla}_k^2 = \begin{bmatrix} -\left(\dfrac{k\omega}{\nu}\right)^2 & 0 \\ 0 & -\left(\dfrac{k\omega}{\nu}\right)^2 \end{bmatrix}. \tag{12}$$

Substituting expressions (6)–(7) and (9)–(10) in the equations of motion (1) yields

$$\mathbf{M}\left(\left(\mathbf{Q}(t)\boldsymbol{\nabla}^2\right) \otimes \mathbb{I}_n\right) \mathbf{z} + \mathbf{C}\left((\mathbf{Q}(t)\boldsymbol{\nabla}) \otimes \mathbb{I}_n\right) \mathbf{z} + \mathbf{K}\left(\mathbf{Q}(t) \otimes \mathbb{I}_n\right) \mathbf{z} = \left(\mathbf{Q}(t) \otimes \mathbb{I}_n\right) \mathbf{b}. \tag{13}$$

Considering the mixed-product property of the Kronecker tensor product $(\mathbf{A} \otimes \mathbf{B})\,(\mathbf{C} \otimes \mathbf{D}) = (\mathbf{AC}) \otimes (\mathbf{BD})$ yields

$$\mathbf{M}\left(\left(\mathbf{Q}(t)\boldsymbol{\nabla}^2\right) \otimes \mathbb{I}_n\right) = (1 \otimes \mathbf{M})\left(\left(\mathbf{Q}(t)\boldsymbol{\nabla}^2\right) \otimes \mathbb{I}_n\right) = \left(\mathbf{Q}(t)\boldsymbol{\nabla}^2\right) \otimes \mathbf{M} \tag{14}$$

$$\mathbf{C}\left((\mathbf{Q}(t)\boldsymbol{\nabla}) \otimes \mathbb{I}_n\right) = (1 \otimes \mathbf{C})\left((\mathbf{Q}(t)\boldsymbol{\nabla}) \otimes \mathbb{I}_n\right) = (\mathbf{Q}(t)\boldsymbol{\nabla}) \otimes \mathbf{C} \tag{15}$$

$$\mathbf{K}\left(\mathbf{Q}(t) \otimes \mathbb{I}_n\right) = (1 \otimes \mathbf{K})\left(\mathbf{Q}(t) \otimes \mathbb{I}_n\right) = \mathbf{Q}(t) \otimes \mathbf{K}. \tag{16}$$

These expressions are plugged into Eq. (13), which gives

$$\left(\left(\mathbf{Q}(t)\boldsymbol{\nabla}^2\right) \otimes \mathbf{M}\right) \mathbf{z} + \left((\mathbf{Q}(t)\boldsymbol{\nabla}) \otimes \mathbf{C}\right) \mathbf{z} + \left(\mathbf{Q}(t) \otimes \mathbf{K}\right) \mathbf{z} = \left(\mathbf{Q}(t) \otimes \mathbb{I}_n\right) \mathbf{b}. \tag{17}$$

In order to remove the time dependency and to obtain an expression relating the different Fourier coefficients, a Galerkin procedure projects Eq. (17) on the orthogonal trigonometric basis $\mathbf{Q}(t)$

$$\left(\left(\frac{2}{T}\int_0^T \mathbf{Q}^T(t)\mathbf{Q}(t)\,dt\,\nabla^2\right)\otimes\mathbf{M}\right)\mathbf{z}+\left(\left(\frac{2}{T}\int_0^T \mathbf{Q}^T(t)\mathbf{Q}(t)\,dt\,\nabla\right)\otimes\mathbf{C}\right)\mathbf{z} + \ldots\left(\left(\frac{2}{T}\int_0^T \mathbf{Q}^T(t)\mathbf{Q}(t)\,dt\right)\otimes\mathbf{K}\right)\mathbf{z}=\left(\left(\frac{2}{T}\int_0^T \mathbf{Q}^T(t)\mathbf{Q}(t)\,dt\right)\otimes\mathbb{I}_n\right)\mathbf{b} \tag{18}$$

where T is the period of the external force. Considering that

$$\frac{2}{T}\int_0^T \mathbf{Q}^T(t)\mathbf{Q}(t)dt=\mathbb{I}_{2N_H+1} \tag{19}$$

the equations of motion expressed in the frequency domain are eventually obtained

$$\left(\nabla^2\otimes\mathbf{M}\right)\mathbf{z}+\left(\nabla\otimes\mathbf{C}\right)\mathbf{z}+\left(\mathbb{I}_{2N_H+1}\otimes\mathbf{K}\right)\mathbf{z}=\left(\mathbb{I}_{2N_H+1}\otimes\mathbb{I}_n\right)\mathbf{b} \tag{20}$$

or, in a more compact form,

$$\mathbf{h}(\mathbf{z},\omega)\equiv\mathbf{A}(\omega)\mathbf{z}-\mathbf{b}(\mathbf{z})=\mathbf{0} \tag{21}$$

where $\mathbf{A}$ is the $(2N_H+1)\,n\times(2N_H+1)\,n$ matrix describing the linear dynamics

$$\mathbf{A}=\nabla^2\otimes\mathbf{M}+\nabla\otimes\mathbf{C}+\mathbb{I}_{2N_H+1}\otimes\mathbf{K} = \begin{bmatrix} \mathbf{K} & & & & \\ & \mathbf{K}-\left(\frac{\omega}{\nu}\right)^2\mathbf{M} & -\frac{\omega}{\nu}\mathbf{C} & & \\ & \frac{\omega}{\nu}\mathbf{C} & \mathbf{K}-\left(\frac{\omega}{\nu}\right)^2\mathbf{M} & & \\ & & & \ddots & \\ & & & \mathbf{K}-\left(N_H\frac{\omega}{\nu}\right)^2\mathbf{M} & -N_H\frac{\omega}{\nu}\mathbf{C} \\ & & & N_H\frac{\omega}{\nu}\mathbf{C} & \mathbf{K}-\left(N_H\frac{\omega}{\nu}\right)^2\mathbf{M} \end{bmatrix}. \tag{22}$$

Expression (21) can be seen as the equations of amplitude of (1), i.e., if $\mathbf{z}^*$ is a root of (21), then the time signals $\mathbf{x}^*$ constructed from $\mathbf{z}^*$ with (2) are solutions of (1).

2.2. Analytical expression of the nonlinear terms and of the Jacobian matrix of the system

Eq. (21) is nonlinear and has to be solved iteratively (e.g., with a Newton–Raphson procedure, or with the hybrid Powell nonlinear solver [67,68]). At each iteration, an evaluation of $\mathbf{b}$ and of $\partial\mathbf{h}/\partial\mathbf{z}$ has to be provided. When $\mathbf{f}$ can be accurately approximated with a few number of harmonics and when its analytical sinusoidal expansion is known [31], or for some types of restoring force [38], analytical expressions relating the Fourier coefficients of the forces $\mathbf{b}$ and of the displacements $\mathbf{z}$ can be obtained together with the expression of the Jacobian matrix of the system. Otherwise, the alternating frequency/time-domain (AFT) technique [15] can be used to compute $\mathbf{b}$:

$$\mathbf{z}\xrightarrow{\text{FFT}^{-1}}\mathbf{x}(t)\rightarrow\mathbf{f}(\mathbf{x},\dot{\mathbf{x}},\omega,t)\xrightarrow{\text{FFT}}\mathbf{b}(\mathbf{z}). \tag{23}$$

The Jacobian matrix of the system can then be computed through finite differences, which is computationally demanding.

An efficient alternative consists in rewriting the inverse Fourier transform as a linear operator $\boldsymbol{\Gamma}(\omega)$. First proposed by Hwang [69], the method, also called *trigonometric collocation*, was adapted to the AFT technique [70], and has been widely used since then [61,71–73]. Denoting N as the number of time samples of a discretized period

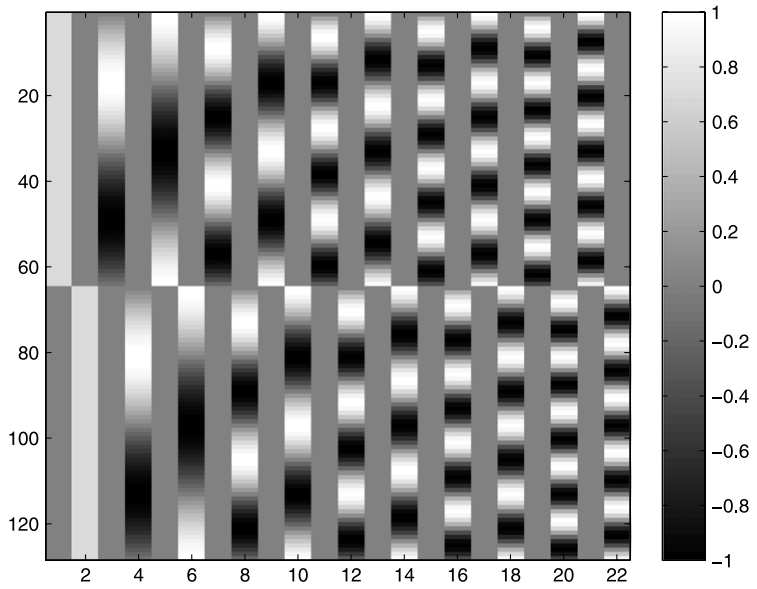

Fig. 1. Illustration of the inverse Fourier transformation matrix $\boldsymbol{\Gamma}(\omega)$ for $n = 2$, $N = 64$, and $N_H = 5$.

of oscillation, one defines vectors $\tilde{\mathbf{x}}$ and $\tilde{\mathbf{f}}$ containing the concatenated nN time samples of the displacements and the forces, respectively, for all DOFs:

$$\tilde{\mathbf{x}} = \begin{bmatrix} x_1(t_1) & \dots & x_1(t_N) & \dots & x_n(t_1) & \dots & x_n(t_N) \end{bmatrix}^T \tag{24}$$

$$\tilde{\mathbf{f}} = \begin{bmatrix} f_1(t_1) & \dots & f_1(t_N) & \dots & f_n(t_1) & \dots & f_n(t_N) \end{bmatrix}^T. \tag{25}$$

The inverse Fourier transform can then be written as a linear operation:

$$\tilde{\mathbf{x}} = \boldsymbol{\Gamma}(\omega)\,\mathbf{z} \tag{26}$$

with the $nN \times (2N_H + 1)\,n$ sparse operator

$$\boldsymbol{\Gamma}(\omega) = \begin{bmatrix} \mathbb{I}_n \otimes \begin{bmatrix} 1/\sqrt{2} \\ 1/\sqrt{2} \\ \vdots \\ 1/\sqrt{2} \end{bmatrix} & \mathbb{I}_n \otimes \begin{bmatrix} \sin\left(\frac{\omega t_1}{\nu}\right) \\ \sin\left(\frac{\omega t_2}{\nu}\right) \\ \vdots \\ \sin\left(\frac{\omega t_N}{\nu}\right) \end{bmatrix} & \mathbb{I}_n \otimes \begin{bmatrix} \cos\left(\frac{\omega t_1}{\nu}\right) \\ \cos\left(\frac{\omega t_2}{\nu}\right) \\ \vdots \\ \cos\left(\frac{\omega t_N}{\nu}\right) \end{bmatrix} & \dots \\ \mathbb{I}_n \otimes \begin{bmatrix} \sin\left(N_H \frac{\omega t_1}{\nu}\right) \\ \sin\left(N_H \frac{\omega t_2}{\nu}\right) \\ \vdots \\ \sin\left(N_H \frac{\omega t_N}{\nu}\right) \end{bmatrix} & \mathbb{I}_n \otimes \begin{bmatrix} \cos\left(N_H \frac{\omega t_1}{\nu}\right) \\ \cos\left(N_H \frac{\omega t_2}{\nu}\right) \\ \vdots \\ \cos\left(N_H \frac{\omega t_N}{\nu}\right) \end{bmatrix} \end{bmatrix}. \tag{27}$$

Fig. 1 represents the inverse transformation matrix for the case $n = 2$, $N = 64$, and $N_H = 5$.
The direct Fourier transformation is written

$$\mathbf{z} = (\boldsymbol{\Gamma}(\omega))^{+}\,\tilde{\mathbf{x}} \tag{28}$$

where $^+$ stands for the Moore–Penrose pseudoinverse $\boldsymbol{\Gamma}^+ = \boldsymbol{\Gamma}^T \left(\boldsymbol{\Gamma}\boldsymbol{\Gamma}^T\right)^{-1}$. The Fourier coefficients of the external and nonlinear forces are simply obtained by transforming the signals in the time domain back to the frequency domain:

$$\mathbf{b}(\mathbf{z}) = \left(\boldsymbol{\Gamma}\left(\omega\right)\right)^+ \tilde{\mathbf{f}}. \tag{29}$$

The Jacobian matrix of expression (21) with respect to the Fourier coefficients $\mathbf{z}$, denoted as $\mathbf{h}_z$, can be computed as in [61,71,73]

$$\mathbf{h}_z = \frac{\partial \mathbf{h}}{\partial \mathbf{z}} = \mathbf{A} - \frac{\partial \mathbf{b}}{\partial \mathbf{z}} = \mathbf{A} - \frac{\partial \mathbf{b}}{\partial \tilde{\mathbf{f}}} \frac{\partial \tilde{\mathbf{f}}}{\partial \tilde{\mathbf{x}}} \frac{\partial \tilde{\mathbf{x}}}{\partial \mathbf{z}} = \mathbf{A} - \boldsymbol{\Gamma}^+ \frac{\partial \tilde{\mathbf{f}}}{\partial \tilde{\mathbf{x}}} \boldsymbol{\Gamma}. \tag{30}$$

In general, the derivatives of the forces with respect to the displacements in the time domain can be expressed analytically, which leads to a very effective computation of the Jacobian matrix. These derivatives have to be evaluated only for the nonlinear DOFs.

2.3. Continuation procedure

Usually, the frequency response is to be computed in a range of frequencies, rather than for a single frequency ω. In this paper, a continuation procedure based on tangent predictions and Moore–Penrose corrections, as in the software MATCONT [7], is coupled to HB. The search for a tangent vector $\mathbf{t}^{(i)}$ at an iteration point $\left(\mathbf{z}^{(i)}, \omega^{(i)}\right)$ along the branch reads

$$\begin{bmatrix} \mathbf{h}_z & \mathbf{h}_\omega \\ \mathbf{t}_{(i-1)}^T & \end{bmatrix} \mathbf{t}_{(i)} = \begin{bmatrix} \mathbf{0} \\ 1 \end{bmatrix} \tag{31}$$

where $\mathbf{h}_\omega$ stands for the derivative of $\mathbf{h}$ with respect to ω,

$$\mathbf{h}_\omega = \frac{\partial \mathbf{h}}{\partial \omega} = \frac{\partial \mathbf{A}}{\partial \omega}\mathbf{z}. \tag{32}$$

The last equation in (31) prevents the continuation procedure from turning back. For the first iteration of the procedure, the sum of the components of the tangent is imposed to be equal to 1.

The correction stage is based on Newton's method. Introducing new optimization variables $\mathbf{v}_{(i,j)}$ initialized as $\mathbf{v}_{(i,1)} = \mathbf{t}_{(i)}$, and $\mathbf{y}_{(i,j)} = \left[\mathbf{z}_{(i,j)}\ \omega_{(i,j)}\right]^T$, the Newton iterations are constructed as follows:

$$\begin{aligned} \mathbf{y}_{(i,j+1)} &= \mathbf{y}_{(i,j)} - \mathbf{G}_y^{-1}\left(\mathbf{y}_{(i,j)}, \mathbf{v}_{(i,j)}\right) \mathbf{G}\left(\mathbf{y}_{(i,j)}, \mathbf{v}_{(i,j)}\right) \\ \mathbf{v}_{(i,j+1)} &= \mathbf{v}_{(i,j)} - \mathbf{G}_y^{-1}\left(\mathbf{y}_{(i,j)}, \mathbf{v}_{(i,j)}\right) \mathbf{R}\left(\mathbf{y}_{(i,j)}, \mathbf{v}_{(i,j)}\right) \end{aligned} \tag{33}$$

with

$$\mathbf{G}\left(\mathbf{y}, \mathbf{v}\right) = \begin{bmatrix} \mathbf{h}\left(\mathbf{y}\right) \\ \mathbf{0} \end{bmatrix}, \qquad \mathbf{G}_y\left(\mathbf{y}, \mathbf{v}\right) = \begin{bmatrix} \mathbf{h}_z\left(\mathbf{y}\right) & \mathbf{h}_\omega\left(\mathbf{y}\right) \\ \mathbf{v}^T & \end{bmatrix}, \qquad \mathbf{R}\left(\mathbf{y}, \mathbf{v}\right) = \begin{bmatrix} \begin{bmatrix} \mathbf{h}_z\left(\mathbf{y}\right) & \mathbf{h}_\omega\left(\mathbf{y}\right) \end{bmatrix} \mathbf{v} \\ \mathbf{0} \end{bmatrix}. \tag{34}$$

3. Harmonic balance for bifurcation detection and tracking

3.1. Stability analysis

The continuation procedure presented in Section 2 does not indicate if a periodic solution is stable or not. In the case of time-domain methods, such as the shooting technique, a by-product of the continuation procedure is the monodromy matrix of the system [3]. Its eigenvalues are termed the *Floquet multipliers* from which the stability of the solution can be deduced. For frequency-domain techniques, one can use a variant of the Floquet theory, the so-called *Hill's method*, whose coefficients are also obtained as a by-product of the calculations. Hill's method is known to give accurate results for a reasonable number of harmonics N_H, and to be effective for large systems [74].

Following the procedure described in [21], a periodic solution $\mathbf{x}^*(t)$ satisfying (1) is perturbed with a periodic solution $\mathbf{s}(t)$ modulated by an exponential decay:

$$\mathbf{p}(t) = \mathbf{x}^*(t) + e^{\lambda t}\mathbf{s}(t). \tag{35}$$

Introducing this perturbation into expression (1) yields

$$\mathbf{M}\ddot{\mathbf{x}}^* + \mathbf{C}\dot{\mathbf{x}}^* + \mathbf{K}\mathbf{x}^* + \left(\lambda^2\mathbf{M}\mathbf{s} + \lambda\left(2\mathbf{M}\dot{\mathbf{s}} + \mathbf{C}\mathbf{s}\right) + \mathbf{M}\ddot{\mathbf{s}} + \mathbf{C}\dot{\mathbf{s}} + \mathbf{K}\mathbf{s}\right)e^{\lambda t} = \mathbf{f}\left(\mathbf{p}, \dot{\mathbf{p}}, \omega, t\right). \tag{36}$$

By approximating the solution and the perturbation as Fourier series truncated to the N_Hth order, i.e., $\mathbf{x}^*(t) = \left(\mathbf{Q}(t) \otimes \mathbb{I}_n\right)\mathbf{z}^*$ and $\mathbf{s}(t) = \left(\mathbf{Q}(t) \otimes \mathbb{I}_n\right)\mathbf{u}$, and by applying a Galerkin procedure as in Section 2.1, we obtain

$$\mathbf{A}\mathbf{z}^* + \left(\boldsymbol{\Delta}_2\lambda^2 + \boldsymbol{\Delta}_1\lambda + \mathbf{A}\right)e^{\lambda t}\mathbf{u} = \mathbf{b}\left(\mathbf{z}^* + e^{\lambda t}\mathbf{u}\right) \tag{37}$$

with

$$\begin{aligned}\boldsymbol{\Delta}_1 &= \nabla \otimes 2\mathbf{M} + \mathbb{I}_{2N_H+1} \otimes \mathbf{C} \\ &= \begin{bmatrix} \mathbf{C} & & & & \\ & \mathbf{C} & -2\frac{\omega}{\nu}\mathbf{M} & & \\ & 2\frac{\omega}{\nu}\mathbf{M} & \mathbf{C} & & \\ & & & \ddots & \\ & & & \mathbf{C} & -2N_H\frac{\omega}{\nu}\mathbf{M} \\ & & & 2N_H\frac{\omega}{\nu}\mathbf{M} & \mathbf{C} \end{bmatrix}\end{aligned} \tag{38}$$

$$\boldsymbol{\Delta}_2 = \mathbb{I}_{2N_H+1} \otimes \mathbf{M}. \tag{39}$$

The right-hand side of Eq. (37) is evaluated through a Taylor series expansion around the solution $\mathbf{z}^*$

$$\mathbf{b}\left(\mathbf{z}^* + e^{\lambda t}\mathbf{u}\right) = \mathbf{b}\left(\mathbf{z}^*\right) + \left.\frac{\partial \mathbf{b}}{\partial \mathbf{z}}\right|_{\mathbf{z}=\mathbf{z}^*}\left(e^{\lambda t}\mathbf{u}\right). \tag{40}$$

Since $\mathbf{A}\mathbf{z}^* - \mathbf{b}\left(\mathbf{z}^*\right)$ is equal to zero by definition, and given that

$$\mathbf{A} - \left.\frac{\partial \mathbf{b}}{\partial \mathbf{z}}\right|_{\mathbf{z}=\mathbf{z}^*} = \mathbf{h}_z \tag{41}$$

replacing (40) in (37) yields

$$\left(\boldsymbol{\Delta}_2\lambda^2 + \boldsymbol{\Delta}_1\lambda + \mathbf{h}_z\right)e^{\lambda t}\mathbf{u} = \mathbf{0}. \tag{42}$$

Hill's coefficients $\boldsymbol{\lambda}$ are thus the solutions of the quadratic eigenvalue problem

$$\boldsymbol{\Delta}_2\lambda^2 + \boldsymbol{\Delta}_1\lambda + \mathbf{h}_z = \mathbf{0}. \tag{43}$$

When embedded in a continuation scheme, $\mathbf{h}_z$ is already obtained from the correction stage ((33)–(34)). Since $\boldsymbol{\Delta}_1$ and $\boldsymbol{\Delta}_2$ are easily computed, the main computational effort amounts to solving a quadratic eigenvalue problem, which can be rewritten as a linear eigenvalue problem of double size

$$\mathbf{B}_1 - \gamma\mathbf{B}_2 = \mathbf{0} \tag{44}$$

with

$$\mathbf{B}_1 = \begin{bmatrix} \boldsymbol{\Delta}_1 & \mathbf{h}_z \\ -\mathbb{I} & \mathbf{0} \end{bmatrix}, \qquad \mathbf{B}_2 = -\begin{bmatrix} \boldsymbol{\Delta}_2 & \mathbf{0} \\ \mathbf{0} & \mathbb{I} \end{bmatrix}. \tag{45}$$

The coefficients $\boldsymbol{\lambda}$ are found among the eigenvalues of the $(2N_H+1)\,2n \times (2N_H+1)\,2n$ matrix

$$\mathbf{B} = \mathbf{B}_2^{-1}\mathbf{B}_1 \tag{46}$$

$$= \begin{bmatrix} -\boldsymbol{\Delta}_2^{-1}\boldsymbol{\Delta}_1 & -\boldsymbol{\Delta}_2^{-1}\mathbf{h}_z \\ \mathbb{I} & \mathbf{0} \end{bmatrix}. \tag{47}$$

However, only $2n$ eigenvalues among the complete set $\boldsymbol{\lambda}$ approximate the Floquet exponents $\tilde{\boldsymbol{\lambda}}$ of the solution $\mathbf{x}^*$ [63]. The other eigenvalues are spurious and do not have any physical meaning; their number also increases with the number of harmonics N_H. Moore [75] showed that the Floquet exponents $\tilde{\boldsymbol{\lambda}}$ are the $2n$ eigenvalues with the smallest imaginary part in modulus. The diagonal matrix

$$\tilde{\mathbf{B}} = \begin{bmatrix} \tilde{\lambda}_1 & & & \\ & \tilde{\lambda}_2 & & \\ & & \ddots & \\ & & & \tilde{\lambda}_{2n} \end{bmatrix} \tag{48}$$

gathers the Floquet exponents and will play a key role for the detection and tracking of bifurcations in Sections 3.2 and 3.3.

Eventually, the stability of a periodic solution can be assessed, i.e., if at least one of the Floquet exponents has a positive real part, then the solution is unstable, otherwise it is asymptotically stable.

3.2. Detection of bifurcations

To detect bifurcations, *test functions* ϕ are evaluated at each iteration of the numerical continuation process [7]. The roots of these test functions indicate the presence of bifurcations.

A fold bifurcation is simply detected when the i_ω-th component of the tangent prediction related to the active parameter ω changes sign [76]. A suitable test function is thus

$$\phi_F = \mathbf{t}_{i_\omega}. \tag{49}$$

According to its algebraic definition [77], we note that a fold bifurcation is characterized by a rank deficiency of 1 of the Jacobian matrix $\mathbf{h}_z$, with $\mathbf{h}_\omega \notin \text{range}\,(\mathbf{h}_z)$. Another (more computationally demanding) test function is therefore

$$\phi_F = |\mathbf{h}_z|\,. \tag{50}$$

Similarly, the Jacobian matrix is rank deficient for branch point (BP) bifurcations, with $\mathbf{h}_\omega \in \text{range}\,(\mathbf{h}_z)$. They can be detected using the test function for fold bifurcations (50), but a more specific test function is [76]

$$\phi_{BP} = \begin{vmatrix} \mathbf{h}_z & \mathbf{h}_\omega \\ \mathbf{t}^T & \end{vmatrix}. \tag{51}$$

The Neimark–Sacker (NS) bifurcation is the third bifurcation studied in this paper. It is detected when a pair of Floquet exponents crosses the imaginary axis as a pair of complex conjugates. According to [78], the bialternate product of a $m \times m$ matrix $\mathbf{P}$, $\mathbf{P}_\odot = \mathbf{P} \odot \mathbb{I}_m$, has a dimension $m(m-1)/2$ and has the property to be singular when two eigenvalues of $\mathbf{P}$ are two purely imaginary complex conjugates. As a result, the test function for NS bifurcations is

$$\phi_{NS} = \left|\tilde{\mathbf{B}}_\odot\right|. \tag{52}$$

The size of the bialternate product rapidly increases with the number of DOFs n, but the diagonal shape of $\tilde{\mathbf{B}}$ implies that $\tilde{\mathbf{B}}_\odot$ is also diagonal, which allows for a fast evaluation of its terms.

To overcome the issue of computing determinants for large-scale systems, the so-called *bordering technique* replaces the evaluation of the determinant of a matrix $\mathbf{G}$ with the evaluation of a scalar function g which vanishes at the same time as the determinant [79]. The function g is obtained by solving the bordered system

$$\begin{bmatrix} \mathbf{G} & \mathbf{p} \\ \mathbf{q}^* & 0 \end{bmatrix} \begin{bmatrix} \mathbf{w} \\ g \end{bmatrix} = \begin{bmatrix} \mathbf{0} \\ 1 \end{bmatrix} \tag{53}$$

where * denotes conjugate transpose, and vectors $\mathbf{p}$ and $\mathbf{q}$ are chosen to ensure the nonsingularity of the system of equations. When $\mathbf{G}$ is almost singular, $\mathbf{p}$ and $\mathbf{q}$ are chosen close to the null vectors of $\mathbf{G}^*$ and $\mathbf{G}$, respectively. For instance, for NS bifurcations $\mathbf{G} = \tilde{\mathbf{B}}_\odot$.

3.3. Tracking of bifurcations

Once a bifurcation is detected, it can be tracked with respect to an additional parameter. To continue codimension-1 bifurcations with respect to two parameters, such as, e.g., the frequency and amplitude of the external forcing, the equation defining the bifurcation $g = 0$ is appended to (21)

$$\begin{cases} \mathbf{h} \equiv \mathbf{A}\mathbf{z} - \mathbf{b} = 0 \\ g = 0. \end{cases} \tag{54}$$

For fold and BP bifurcations, g is the solution of the bordered system (53) with $\mathbf{G} = \mathbf{h}_z$. For NS bifurcations, $\mathbf{G} = \tilde{\mathbf{B}}_\odot$ is considered in the bordered system.

During the continuation procedure, the computation of the derivatives of the additional equation is required. As shown in [79], analytical expressions for the derivatives of g with respect to α, where α denotes a component of $\mathbf{z}$ or one of the two active parameters, are found as

$$g_\alpha = -\mathbf{v}^* \mathbf{G}_\alpha \mathbf{w} \tag{55}$$

where $\mathbf{G}_\alpha$ is the derivative of $\mathbf{G}$ with respect to α, and where $\mathbf{w}$ and $\mathbf{v}$ comes from the resolution of the bordered system and its transposed version:

$$\begin{bmatrix} \mathbf{G} & \mathbf{p} \\ \mathbf{q}^* & 0 \end{bmatrix} \begin{bmatrix} \mathbf{w} \\ g \end{bmatrix} = \begin{bmatrix} \mathbf{0} \\ 1 \end{bmatrix} \tag{56}$$

$$\begin{bmatrix} \mathbf{G} & \mathbf{p} \\ \mathbf{q}^* & 0 \end{bmatrix}^* \begin{bmatrix} \mathbf{v} \\ e \end{bmatrix} = \begin{bmatrix} \mathbf{0} \\ 1 \end{bmatrix}. \tag{57}$$

As a result, the only term that has to be evaluated is $\mathbf{G}_\alpha$. For fold and BP bifurcations,

$$\mathbf{G}_\alpha = \mathbf{h}_{z\alpha} \tag{58}$$

where $\mathbf{h}_{z\alpha}$ is the derivative of the Jacobian $\mathbf{h}_z$ with respect to α and is computed through finite differences.

For NS bifurcations,

$$\mathbf{G}_\alpha = \frac{\partial}{\partial \alpha}\left(\tilde{\mathbf{B}}_\odot\right) = \left(\frac{\partial}{\partial \alpha}\left(\tilde{\mathbf{B}}\right)\right)_\odot = \begin{bmatrix} \frac{\partial \tilde{\lambda}_1}{\partial \alpha} & & & \\ & \frac{\partial \tilde{\lambda}_2}{\partial \alpha} & & \\ & & \ddots & \\ & & & \frac{\partial \tilde{\lambda}_{2n}}{\partial \alpha} \end{bmatrix}_\odot . \tag{59}$$

Finite differences could be used to compute the derivatives of the Floquet exponents. However, this means that the eigenvalue problem (44) has to be solved for each perturbation of the components of $\mathbf{z}$, and for the perturbation of the two continuation parameters. This represents a total of $n\,(2N_H + 1) + 2$ resolutions of the eigenvalue problem per iteration, which is cumbersome for large systems. Instead, we propose to compute the derivatives in (59) using the properties of eigenvalue derivatives demonstrated by Van der Aa et al. [80]. Denoting as $\boldsymbol{\Lambda}$ the eigenvector matrix of $\mathbf{B}$, and $\boldsymbol{\xi}$ the localization vector containing the index of the $2n$ Floquet exponents $\tilde{\boldsymbol{\lambda}}$ among the eigenvalues $\boldsymbol{\lambda}$, i.e., $\tilde{\lambda}_i = \lambda_{\xi_i}$, the eigenvalues derivatives can be computed as

$$\frac{\partial \tilde{\lambda}_i}{\partial \alpha} = \left(\boldsymbol{\Lambda}^{-1} \frac{\partial \mathbf{B}}{\partial \alpha} \boldsymbol{\Lambda}\right)_{(\xi_i, \xi_i)} . \tag{60}$$

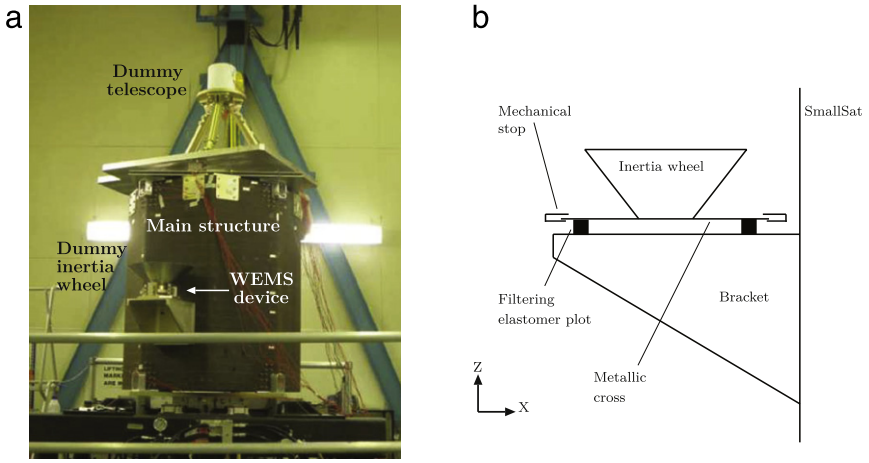

Fig. 2. SmallSat spacecraft. (a) Photograph; (b) Schematic of the WEMS, the nonlinear vibration isolation device.

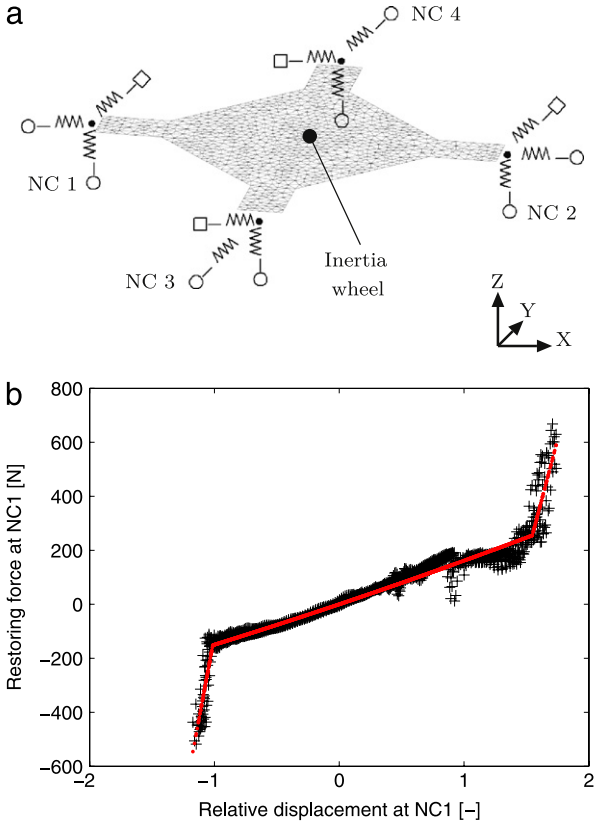

Fig. 3. WEMS. (a) Modeling of the device using shell elements, a point mass, linear and nonlinear springs. The linear and nonlinear springs are represented with squares and circles, respectively. (b) Identified stiffness curve of NC1 (in black) and fitting with a trilinear model (in red). (For interpretation of the references to color in this figure legend, the reader is referred to the web version of this article.)

An analytical expression relating the derivative of $\mathbf{B}$ with respect to α in function of $\mathbf{h}_{z\alpha}$ can be obtained from Eq. (47). As for fold and BP bifurcations, $\mathbf{h}_{z\alpha}$ is computed through finite differences.

From the computational viewpoint, the evaluation of the $(2N_H + 1)\, n + 2$ terms g_α represents the main burden of the method when there is a large number of nonlinear DOFs (e.g., in the case of distributed nonlinearities). In this

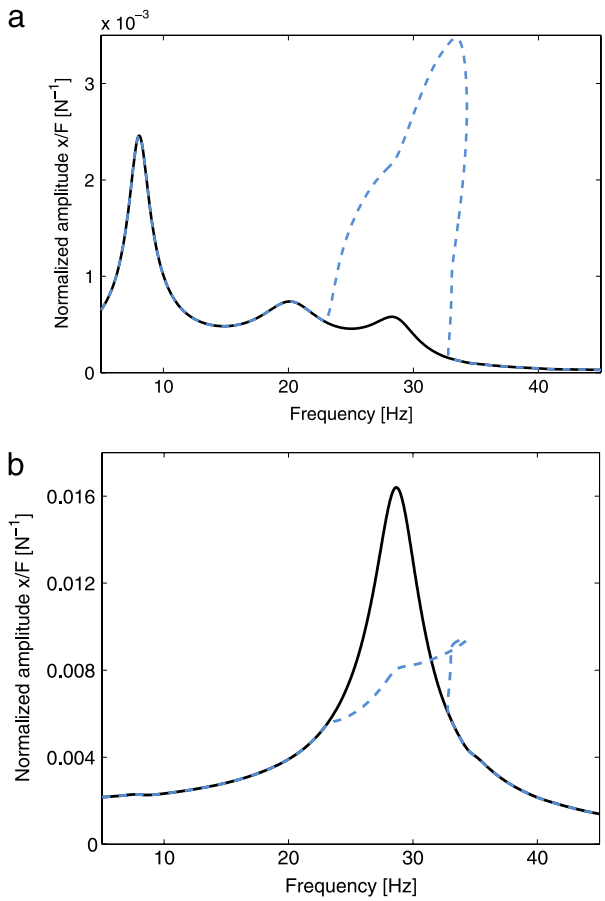

Fig. 4. Normalized frequency response at NC1. (a) NC1-X; (b) NC1-Z. The solid and dashed lines represent forcing amplitude of $F = 50$ N and $F = 155$ N, respectively.

case, parallel computing could help reduce the computational cost of the algorithm. For localized nonlinearities, one can take advantage of the fact that $\mathbf{h}_{z\alpha}$ is a null matrix when α corresponds to Fourier coefficients of linear DOFs.

4. Bifurcation analysis of a satellite structure

4.1. Description of the SmallSat spacecraft

The effectiveness of the proposed HB method is demonstrated using the *SmallSat*, a spacecraft structure conceived by EADS-Astrium (now Airbus Defence and Space). The spacecraft is 1.2 m in height and 1 m in width. A prototype of the spacecraft with a dummy telescope is represented in Fig. 2(a). The nonlinear component, the so-called *wheel elastomer mounting system* (WEMS), is mounted on a bracket connected to the main structure and loaded with an 8-kg dummy inertia wheel, as depicted in Fig. 2(b). The WEMS device acts as mechanical filter which mitigates the on-orbit micro-vibrations of the inertia wheel through soft elastomer plots located between the metallic cross that supports the inertia wheel and the bracket. To avoid damage of the elastomer plots during launch, the axial and lateral motions of the metallic cross are limited by four nonlinear connections labeled NC1 – 4. Each NC comprises two mechanical stops that are covered with a thin layer of elastomer to prevent metal–metal impacts.

A finite element model (FEM) was built to conduct numerical experiments. Linear shell elements were used for the main structure and the instrument baseplate, and a point mass represented the dummy telescope. Proportional damping was considered for these components. As shown in Fig. 3(a), the metallic cross of the WEMS was also modeled using linear shell elements whereas the inertia wheel was seen as a point mass owing to its important rigidity. To achieve tractable calculations, the linear elements of the FEM were condensed using the Craig–Bampton reduction technique.

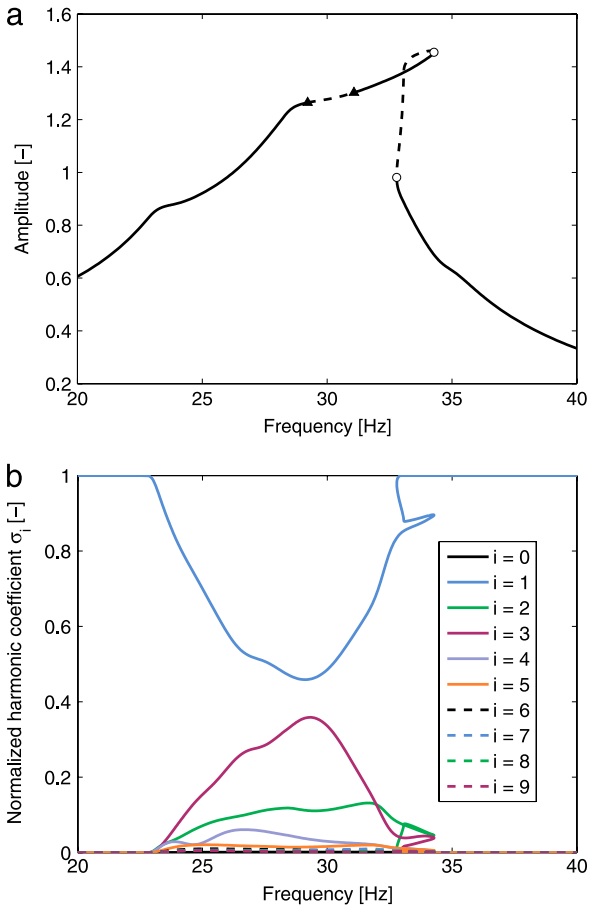

Fig. 5. Frequency response at NC1-Z for $F = 155$ N. (a) Displacement. Circle and triangle markers represent fold and NS bifurcations, respectively. The solid and dashed lines represent stable and unstable solutions, respectively. (b) Harmonic coefficients. (For interpretation of the references to color in this figure legend, the reader is referred to the web version of this article.)

Specifically, the FEM was reduced to 10 internal modes and 9 nodes (excluding DOFs in rotation), namely both sides of each NC and the inertia wheel. In total, the reduced-order model thus contains 37 DOFs.

Each NC was then modeled using a trilinear spring in the axial direction (elastomer in traction/compression plus two stops), a bilinear spring in the radial direction (elastomer in shear plus one stop) and a linear spring in the third direction (elastomer in shear). The values of the spring coefficients were identified from experimental data [81]. For instance, the stiffness curve identified for NC1 is displayed in Fig. 3(b). To avoid numerical issues, regularization with third-order polynomials was utilized in the close vicinity of the clearances to implement C^1 continuity. The dissipation in the elastomer plots was modeled using lumped dashpots. We note that the predictions of the resulting nonlinear model were found in good agreement with experimental data [81,82].

For confidentiality, clearances and displacements are given through a dimensionless quantities throughout the paper.

4.2. *Frequency response, Floquet exponents and bifurcation detection*

The forced response of the satellite for harmonic forcing applied to the vertical DOF of the inertia wheel is computed using HB with $N_H = 9$ harmonics and $N = 1024$ points per period. Fig. 4 depicts the system's frequency response curves at NC1-X and NC1-Z for two forcing amplitudes, $F = 50$ and 155 N. For a clear assessment of the effects of the nonlinearities, the response amplitudes are normalized with the forcing amplitude F in this figure. Because the normalized responses for the two forcing amplitudes coincide up to 23 Hz, one can conclude that the motion is purely linear in this frequency range. Conversely, the mode with a linear resonance frequency of 28.8 Hz

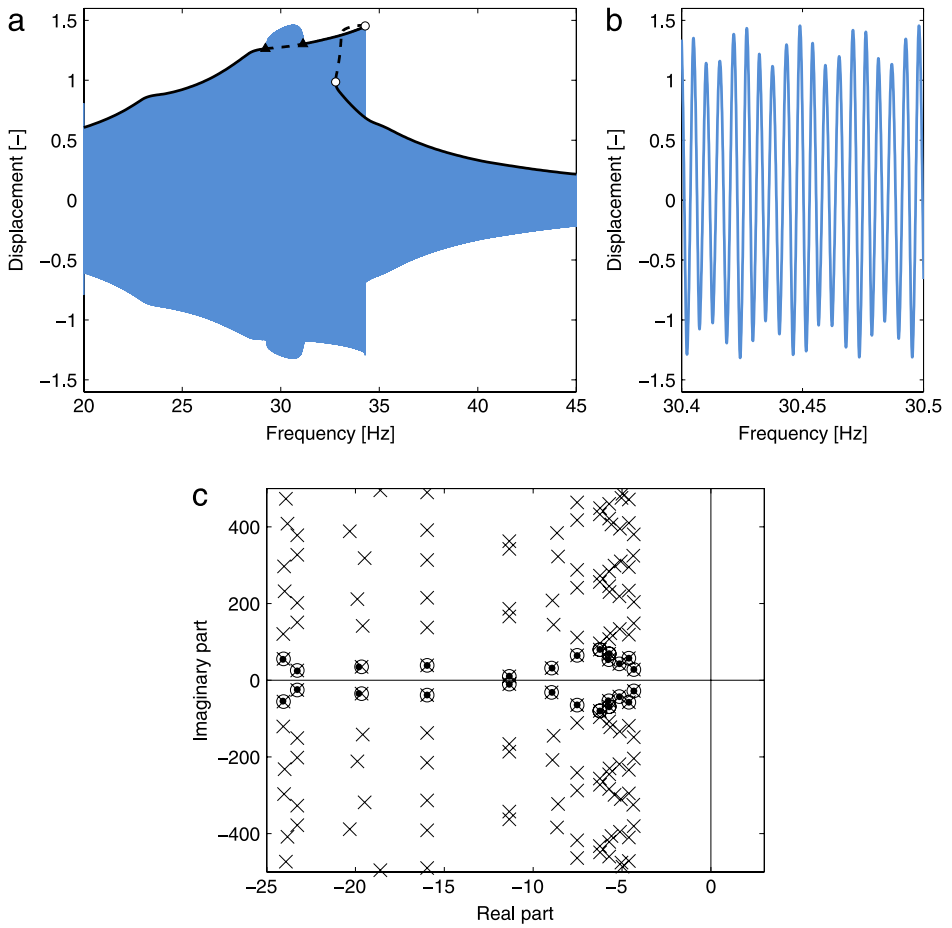

Fig. 6. Bifurcations, quasiperiodic oscillations and Floquet exponents. (a) Comparison between HB (black) and a swept-sine response calculated using Newmark's algorithm (blue) for $F = 155$ N at NC1-Z. Circle and triangle markers depict fold and NS bifurcations, respectively. The solid and dashed lines represent stable and unstable solutions, respectively. (b) Close-up of the quasiperiodic oscillations. (c) Periodic solution at 28 Hz: Hill's coefficients $\boldsymbol{\lambda}$ (crosses), Floquet exponents $\tilde{\boldsymbol{\lambda}}$ obtained with Hill's method (circles), and Floquet exponents $\tilde{\boldsymbol{\lambda}}_{TI}$ obtained from the monodromy matrix (dots). (For interpretation of the references to color in this figure legend, the reader is referred to the web version of this article.)

is greatly affected by the WEMS nonlinearities, which can be explained by the fact that this mode combines bracket deflection with WEMS motion [82].

Fig. 5(a) presents a close-up of this nonlinear resonance at NC1-Z where stability and bifurcations are also indicated. The evolution of the normalized harmonic coefficients

$$\sigma_i = \frac{\phi_i}{\sum_{k=0}^{N_H} \phi_i} \qquad (i = 0, \ldots, N_H) \tag{61}$$

with

$$\phi_0 = \frac{c_0^x}{\sqrt{2}}, \qquad \phi_i = \sqrt{\left(s_i^x\right)^2 + \left(c_i^x\right)^2} \quad (i = 1, \ldots, N_H) \tag{62}$$

is shown in Fig. 5(b). From 20 to 23 Hz, only the fundamental harmonic is present in the response. In the resonance region, the SmallSat nonlinearities activate other harmonics in the response. Even harmonics contribute to the dynamics because of the asymmetric modeling of the NCs of the WEMS. From the figure, it is also clear that the 6th and higher harmonics have a negligible participation in the response; for this reason, $N_H = 5$ is considered throughout the rest of the paper.

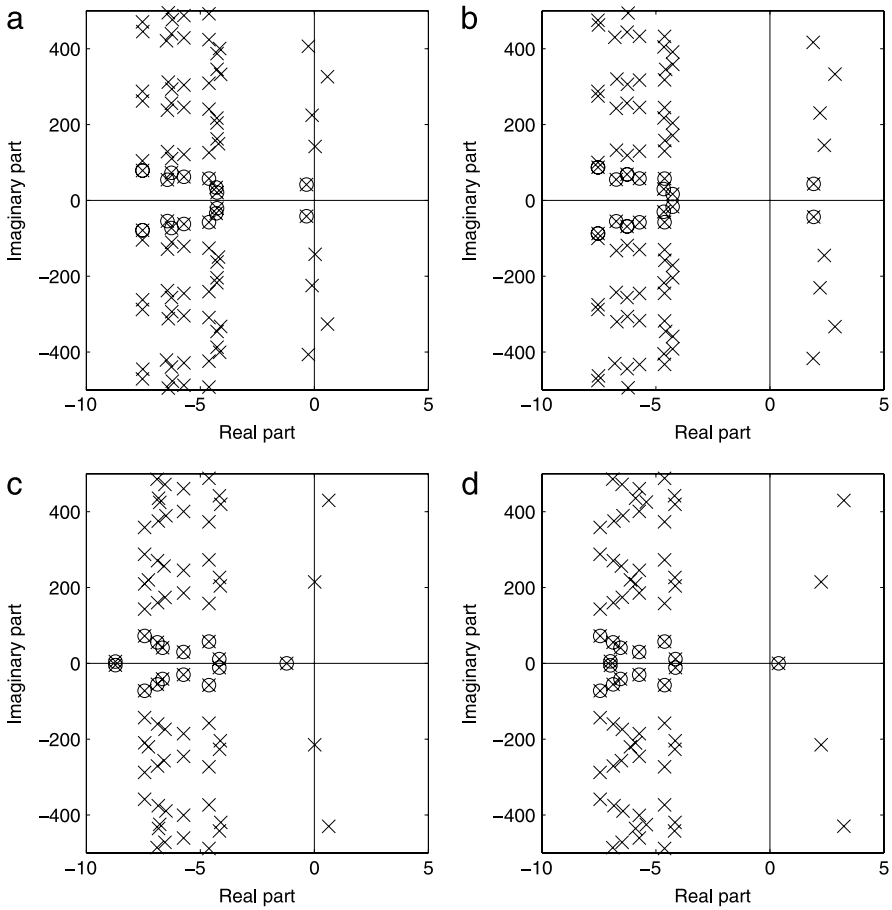

Fig. 7. Floquet exponents in the vicinity of the fold and NS bifurcations. (a) Before the NS bifurcation at $\omega = 29.11$ Hz, stable region. (b) After the NS bifurcation at $\omega = 29.8$ Hz, unstable region. (c) Before the fold bifurcation at $\omega = 34.25$ Hz, stable region. (d) After the fold bifurcation at $\omega = 34.28$ Hz, unstable region. Hill's coefficients $\boldsymbol{\lambda}$ and Floquet exponents $\tilde{\boldsymbol{\lambda}}$ obtained with Hill's method are denoted with crosses and circles, respectively.

The nonlinear resonance has a complex and rich topology. Not only the frequency response curve was found to fold backwards, but bifurcations were detected along the branch by the HB algorithm in Fig. 5(a). Fold bifurcations are generic for nonlinear resonances and are responsible for stability changes. NS bifurcations imply that further investigation of the dynamics should be carried out in the corresponding range of frequencies, because a branch of quasiperiodic solutions bifurcates out from the main branch. To this end, the response to a swept-sine excitation with a forcing amplitude $F = 155$ N and with a sweep rate of 0.5 Hz/min was computed with a Newmark time integration scheme. The sampling frequency was chosen very high, i.e., 3000 Hz, to guarantee the accuracy of the simulation in Fig. 6(a). The first observation is that overall the frequency response computed using HB provides a very accurate estimation of the envelope of the swept-sine response. In addition, a modulation of the displacement's envelope is clearly noticed between the two NS bifurcations highlighted by HB, and the close-up in Fig. 6(b) confirms the presence of quasiperiodic oscillations. Interestingly, the amplitudes associated with these oscillations are slightly larger than those at resonance, which shows the importance of a proper characterization of these oscillations.

Fig. 6(c) shows a subset of Hill's coefficients $\boldsymbol{\lambda}$ and Floquet exponents $\tilde{\boldsymbol{\lambda}}$ obtained with Hill's method ($N_H = 5$ and $N = 1024$) for the stable periodic solution at 28 Hz in Fig. 6(a). Floquet exponents $\tilde{\boldsymbol{\lambda}}_{TI}$ are also calculated from the monodromy matrix evaluated with a Newmark time integration scheme as in [3]; they serve as a reference solution. The comparison demonstrates that the actual Floquet exponents corresponds to the Hill's coefficients that are the closest ones to the real axis, which validates the sorting criterion discussed in Section 3.1. The other coefficients

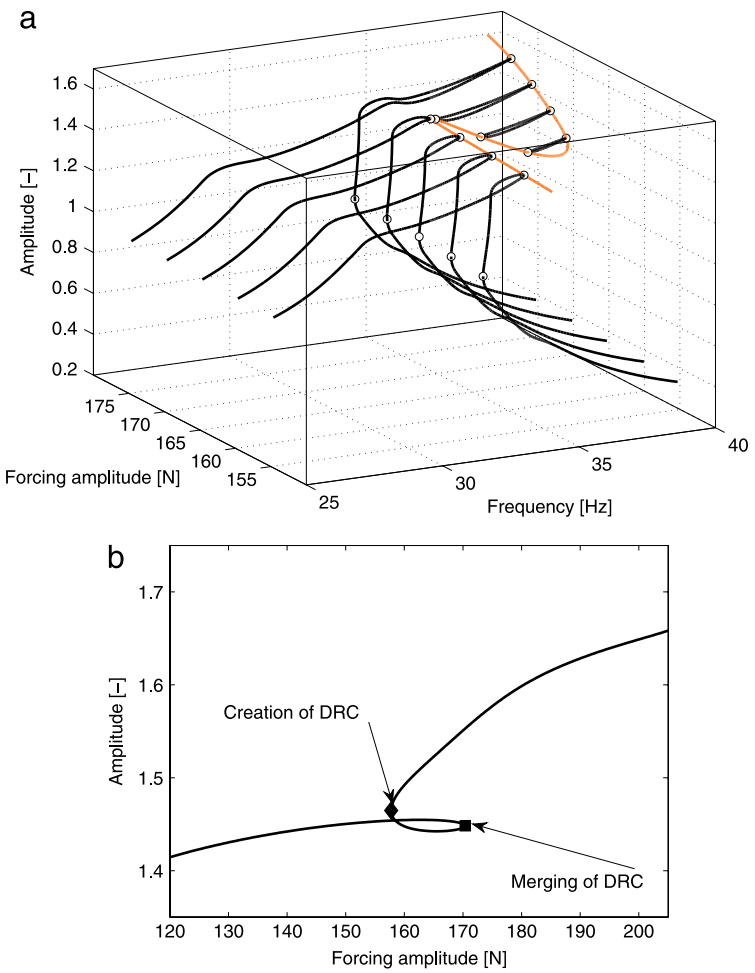

Fig. 8. Tracking of the fold bifurcations of the resonance peak. (a) Three-dimensional space. Orange line: branch of fold bifurcations; black lines: frequency responses at NC1-Z for $F = 155$ N, 160 N, 170 N and 175 N. Circle markers depict fold bifurcations. (b) Two-dimensional projection of the branch of fold bifurcations. (For interpretation of the references to color in this figure legend, the reader is referred to the web version of this article.)

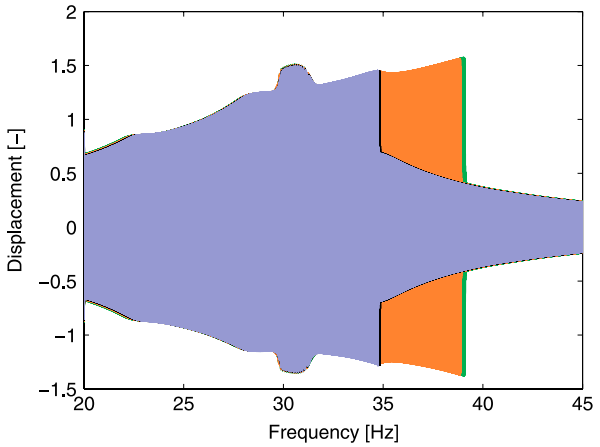

Fig. 9. NC1-Z displacement for swept-sine excitations with $F = 168$ N (purple), 170 N (black), 172 N (orange) and 174 N (green). (For interpretation of the references to color in this figure legend, the reader is referred to the web version of this article.)

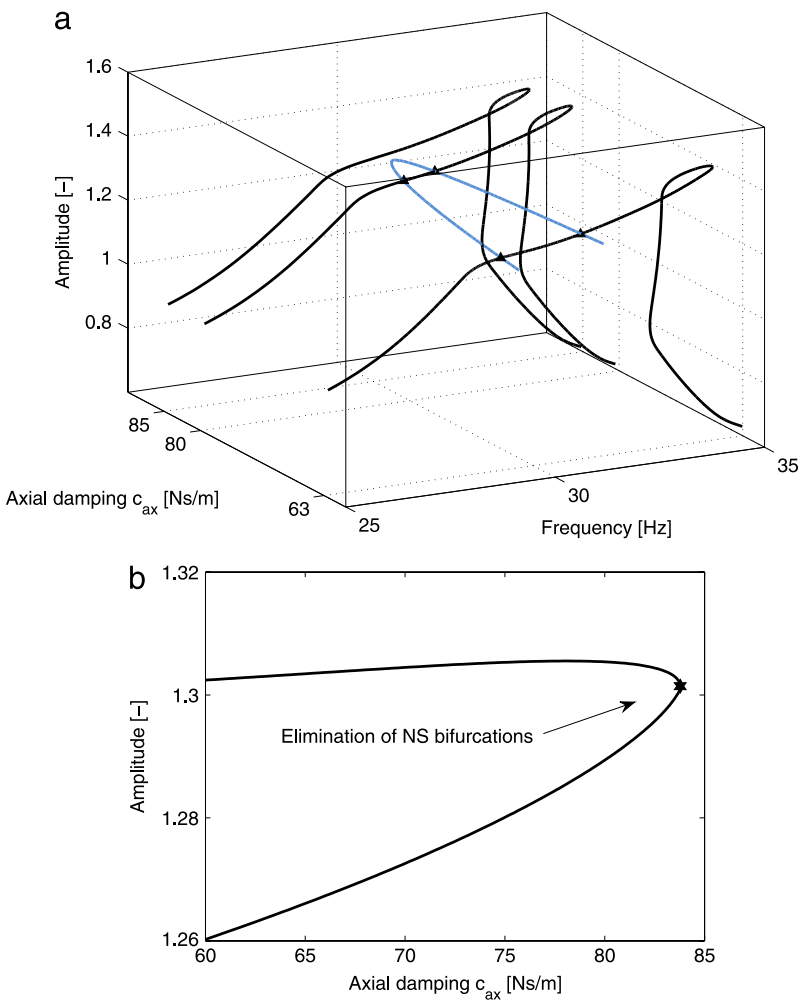

Fig. 10. Tracking of the NS bifurcations. (a) Three-dimensional space. Blue line: branch of NS bifurcations; black lines: frequency responses of the at NC1-Z for $F = 155$ N and for $c_{ax} = 63$ Ns/m, 80 Ns/m and 85 Ns/m. Triangle markers depict NS bifurcations. (b) Two-dimensional projection of the branch of NS bifurcations. (For interpretation of the references to color in this figure legend, the reader is referred to the web version of this article.)

are spurious, but they seem to be aligned according to the same pattern as that of the actual Floquet exponents. The location of all exponents in the left-half plane indicates that the solution at 28 Hz is indeed stable.

The evolution of Hill's coefficients and Floquet exponents in the vicinity of the first NS bifurcation is given in Fig. 7(a–b). Before the bifurcation, the Floquet exponents lie all in the left-half plane in Fig. 7(a), which indicates a stable solution. We stress that a pair of Hill's coefficients has already crossed the imaginary axis in this figure, which evidences that considering all Hill's coefficients can thus lead to misjudgment. After the bifurcation, a pair of complex conjugates Floquet exponents now lie in the right-half plane in Fig. 7(b), which means that the system underwent a NS bifurcation and lost stability. A similar scenario is depicted for the first fold bifurcation in Fig. 7(c–d) with the difference that a single Floquet exponent crosses the imaginary axis through zero.

4.3. Bifurcation tracking

The fold bifurcations revealed in the previous section are now tracked in the codimension-2 forcing frequency-forcing amplitude space using the algorithm presented in Section 3.3. Fig. 8(a) represents the resulting fold curve, together with the frequency responses of the system for different forcing amplitudes. Very interestingly, the algorithm initially tracks the fold bifurcations of the main frequency response, but it then turns back to reveal a *detached*

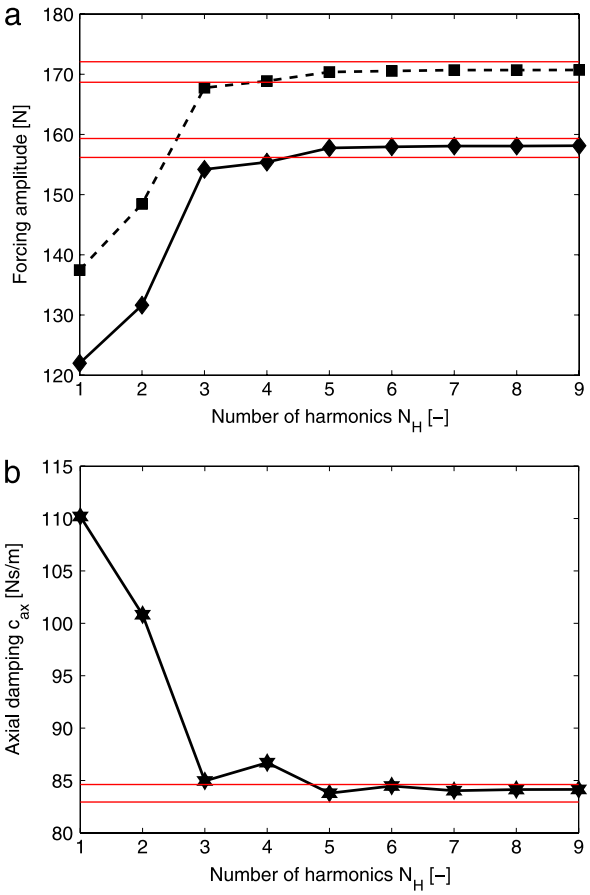

Fig. 11. Convergence of the bifurcation tracking algorithm with respect to the number of harmonics N_H. (a) Fold bifurcations: the solid line with diamond markers corresponds to the creation of the DRC, whereas the dashed line with square markers corresponds to the merging of the DRC with the main resonance. (b) NS bifurcations: the solid line with stars markers corresponds to the elimination of the bifurcations. For both figures, the red lines give $+1\%$ and -1% variations with respect to $N_H = 5$. (For interpretation of the references to color in this figure legend, the reader is referred to the web version of this article.)

resonance curve (DRC), or *isola*. Such an attractor is rarely observed for real structures in the literature. Fig. 8(b), which shows the projection of the fold curve in the forcing amplitude–response amplitude plane, highlights that the DRC is created when $F = 158$ N. The DRC then expands both in frequency and amplitude until $F = 170$ N for which merging with the resonance peak occurs. Because the upper part of the DRC is stable, the resonance peak after the merging is characterized by a greater frequency and amplitude. This merging process is further illustrated in Fig. 9, where the responses to swept-sine excitations of amplitude 168, 170, 172 and 174 N are superimposed. Moving from $F = 170$ N to $F = 172$ N leads to a sudden 'jump' in resonance frequency and amplitude.

Bifurcation tracking is not only useful for understanding the system's dynamics and revealing additional attractors, but it can also be used for engineering design. For instance, we use it herein to study the influence of the axial dashpot c_{ax} of the WEMS device on the quasiperiodic oscillations. Fig. 10(a) depicts the NS curve in the codimension-2 forcing frequency–axial damping space to which frequency responses computed for $c_{ax} = 63$ Ns/m (reference), 80 Ns/m and 85 Ns/m are superimposed. The projection in the c_{ax}-response amplitude plane in Fig. 10(b) shows that the two NS bifurcations, and hence quasiperiodic oscillations, can be completely eliminated for $c_{ax} = 84$ Ns/m.

Finally, the convergence of the algorithm is assessed in Fig. 11, for which the fold and NS curves presented in Figs. 8 and 10 were recomputed for a number of harmonics N_H varying from 1 to 9. In both cases, a clear convergence of the results is observed. These figures also confirm that retaining 5 harmonics in the Fourier series leads to an error less than 1%.

5. Conclusions

The purpose of this paper was to exploit the harmonic balance method for the computation of periodic solutions and their bifurcations in codimension-2 parameter space. Particular attention was devoted to the computational efficiency of the algorithm, which motivated the use of a bordering technique and the development of a new procedure for Neimark–Sacker bifurcations exploiting the properties of eigenvalue derivatives.

The method was demonstrated using a real satellite example possessing several mechanical stops. By combining the proposed algorithm with Craig–Bampton reduction, we showed that bifurcation tracking of large-scale structures with localized nonlinearities is now within reach; it represents a particularly effective tool both for uncovering dynamical attractors and for engineering design.

Acknowledgments

The authors Thibaut Detroux, Luc Masset and Gaetan Kerschen would like to acknowledge the financial support of the European Union (ERC Starting Grant NoVib 307265). The author L. Renson is a Marie-Curie COFUND Postdoctoral Fellow of the University of Liège, co-funded by the European Union.

References

[1] C. Padmanabhan, R. Singh, Analysis of periodically excited non-linear systems by a parametric continuation technique, J. Sound Vib. 184 (1) (1995) 35–58.
[2] S. Stoykov, S. Margenov, Numerical computation of periodic responses of nonlinear large-scale systems by shooting method, Comput. Math. Appl. 367 (5) (2014) 2257–2267.
[3] M. Peeters, R. Viguié, G. Sérandour, G. Kerschen, J.-C. Golinval, Nonlinear normal modes, Part II: Toward a practical computation using numerical continuation techniques, Mech. Syst. Signal Process. 23 (1) (2009) 195–216.
[4] E.J. Doedel, A.R. Champneys, T.F. Fairgrieve, Y.A. Kuznetsov, B. Sandstede, X. Wang, AUTO97: Continuation and bifurcation software for ordinary differential equations (with homcont), in: User's Guide, Concordia University, Montreal, Canada, 1997, Available from http://indy.cs.concordia.ca.
[5] U. Ascher, J. Christiansen, R.D. Russell, A collocation solver for mixed order systems of boundary value problems, Math. Comp. (1979) 659–679.
[6] Y.A. Kuznetsov, V.V. Levitin, CONTENT: A multiplatform environment for analyzing dynamical systems, in: User's Guide, Dynamical Systems Laboratory, CWI, Amsterdam, Netherlands, 1995-1997, Available by anonymous ftp from ftp.cwi.nl/pub/CONTENT.
[7] A. Dhooge, W. Govaerts, Y.A. Kuznetsov, Matcont: a matlab package for numerical bifurcation analysis of odes, ACM Trans. Math. Software 29 (2) (2003) 141–164.
[8] H. Dankowicz, F. Schilder, An extended continuation problem for bifurcation analysis in the presence of constraints, J. Comput. Nonlinear Dyn. 6 (3) (2011).
[9] N.M. Krylov, N.N. Bogoliubov, Introduction to Non-Linear Mechanics, vol. 11, Princeton University Press, 1943.
[10] M. Urabe, Galerkin's procedure for nonlinear periodic systems, Arch. Ration. Mech. Anal. 20 (2) (1965) 120–152.
[11] S. Karkar, B. Cochelin, C. Vergez, A comparative study of the harmonic balance method and the orthogonal collocation method on stiff nonlinear systems, J. Sound Vib. 333 (12) (2014) 2554–2567.
[12] S. Lau, Y. Cheung, Amplitude incremental variational principle for nonlinear vibration of elastic systems, J. Appl. Mech. 48 (4) (1981) 959–964.
[13] Y. Cheung, S. Lau, Incremental time–space finite strip method for non-linear structural vibrations, Earthq. Eng. Struct. Dyn. 10 (2) (1982) 239–253.
[14] K. Sze, S. Chen, J. Huang, The incremental harmonic balance method for nonlinear vibration of axially moving beams, J. Sound Vib. 281 (3) (2005) 611–626.
[15] T. Cameron, J. Griffin, An alternating frequency/time domain method for calculating the steady-state response of nonlinear dynamic systems, J. Appl. Mech. 56 (1) (1989) 149–154.
[16] A. Cardona, A. Lerusse, M. Géradin, Fast fourier nonlinear vibration analysis, Comput. Mech. 22 (2) (1998) 128–142.
[17] J.-J. Sinou, A. Lees, A non-linear study of a cracked rotor, Eur. J. Mech. A 26 (1) (2007) 152–170.
[18] V. Jaumouillé, J.-J. Sinou, B. Petitjean, An adaptive harmonic balance method for predicting the nonlinear dynamic responses of mechanical systems—Application to bolted structures, J. Sound Vib. 329 (19) (2010) 4048–4067.
[19] J. Guillen, C. Pierre, An efficient, hybrid, frequency–time domain method for the dynamics of large-scale dry-friction damped structural systems, in: IUTAM Symposium on Unilateral Multibody Contacts, Springer, 1999, pp. 169–178.
[20] O. Poudou, C. Pierre, Hybrid frequency–time domain methods for the analysis of complex structural systems with dry friction damping, in Collection of Technical Papers—AIAA/ASME/ASCE/AHS/ASC Structures, Structural Dynamics and Materials Conference, 2003, pp. 111–124.
[21] G. von Groll, D.J. Ewins, The harmonic balance method with arc-length continuation in rotor/stator contact problems, J. Sound Vib. 241 (2) (2001) 223–233.

[22] R. Arquier, Une méthode de calcul des modes de vibrations non-linéaires de structures (Ph.D. thesis), Université de la méditerranée Aix-Marseille II, Marseille, France, 2007.
[23] B. Cochelin, C. Vergez, A high order purely frequency-based harmonic balance formulation for continuation of periodic solutions, J. Sound Vib. 324 (1) (2009) 243–262.
[24] A. Grolet, F. Thouverez, On a new harmonic selection technique for harmonic balance method, Mech. Syst. Signal Process. 30 (2012) 43–60.
[25] K.S. Kundert, A. Sangiovanni-Vincentelli, Simulation of nonlinear circuits in the frequency domain, IEEE Trans. Comput.-Aided Des. Integr. Circuits Syst. 5 (4) (1986) 521–535.
[26] R. Genesio, A. Tesi, Harmonic balance methods for the analysis of chaotic dynamics in nonlinear systems, Automatica 28 (3) (1992) 531–548.
[27] S.C. Stanton, B.A. Owens, B.P. Mann, Harmonic balance analysis of the bistable piezoelectric inertial generator, J. Sound Vib. 331 (15) (2012) 3617–3627.
[28] C.-C. Fang, Critical conditions for a class of switched linear systems based on harmonic balance: applications to dc–dc converters, Nonlinear Dynam. 70 (3) (2012) 1767–1789.
[29] S.F. Shen, An approximate analysis of nonlinear flutter problems, J. Aerosp. Sci. 26 (1) (1959) 25–32.
[30] L. Liu, E.H. Dowell, Harmonic balance approach for an airfoil with a freeplay control surface, AIAA J. 43 (4) (2005) 802–815.
[31] B. Lee, L. Liu, K. Chung, Airfoil motion in subsonic flow with strong cubic nonlinear restoring forces, J. Sound Vib. 281 (3) (2005) 699–717.
[32] G. Dimitriadis, Continuation of higher-order harmonic balance solutions for nonlinear aeroelastic systems, J. Aircr. 45 (2) (2008) 523–537.
[33] K.C. Hall, J.P. Thomas, W.S. Clark, Computation of unsteady nonlinear flows in cascades using a harmonic balance technique, AIAA J. 40 (5) (2002) 879–886.
[34] A. Gopinath, E. Van Der Weide, J.J. Alonso, A. Jameson, K. Ekici, K.C. Hall, Three-dimensional unsteady multi-stage turbomachinery simulations using the harmonic balance technique, in: 45th AIAA Aerospace Sciences Meeting and Exhibit, vol. 892, 2007.
[35] S.T. Clark, F.M. Besem, R.E. Kielb, J.P. Thomas, Developing a reduced-order model of nonsynchronous vibration in turbomachinery using proper-orthogonal decomposition methods, J. Eng. Gas Turbines Power 137 (5) (2015) 052501.
[36] K. Ekici, K.C. Hall, E.H. Dowell, Computationally fast harmonic balance methods for unsteady aerodynamic predictions of helicopter rotors, J. Comput. Phys. 227 (12) (2008) 6206–6225.
[37] A. Cardona, T. Coune, A. Lerusse, M. Geradin, A multiharmonic method for non-linear vibration analysis, Int. J. Numer. Methods Eng. 37 (9) (1994) 1593–1608.
[38] E. Petrov, D. Ewins, Analytical formulation of friction interface elements for analysis of nonlinear multi-harmonic vibrations of bladed disks, J. Turbomach. 125 (2) (2003) 364–371.
[39] D. Süß, K. Willner, Investigation of a jointed friction oscillator using the multiharmonic balance method, Mech. Syst. Signal Process. 52 (2015) 73–87.
[40] K.-C. Woo, A.A. Rodger, R.D. Neilson, M. Wiercigroch, Application of the harmonic balance method to ground moling machines operating in periodic regimes, Chaos Solitons Fractals 11 (15) (2000) 2515–2525.
[41] S. Peter, P. Reuss, L. Gaul, Identification of sub-and higher harmonic vibrations in vibro-impact systems, in: Nonlinear Dynamics, vol. 2, Springer, 2014, pp. 131–140.
[42] R. Lewandowski, Computational formulation for periodic vibration of geometrically nonlinear structures—part 2: numerical strategy and examples, Int. J. Solids Struct. 34 (15) (1997) 1949–1964.
[43] P. Ribeiro, M. Petyt, Geometrical non-linear, steady state, forced, periodic vibration of plates, part i: model and convergence studies, J. Sound Vib. 226 (5) (1999) 955–983.
[44] F. Barillon, J.-J. Sinou, J.-M. Duffal, L. Jézéquel, Non-linear dynamics of a whole vehicle finite element model using a harmonic balance method, Int. J. Veh. Des. 63 (4) (2013) 387–403.
[45] A. Sénéchal, B. Petitjean, L. Zoghai, Development of a numerical tool for industrial structures with local nonlinearities, in: Proceedings of the 26th International Conference on Noise and Vibration engineering (ISMA2014), Leuven, Belgium, 2014.
[46] M. Claeys, J.-J. Sinou, J.-P. Lambelin, B. Alcoverro, Multi-harmonic measurements and numerical simulations of nonlinear vibrations of a beam with non-ideal boundary conditions, Commun. Nonlinear Sci. Numer. Simul. (2014).
[47] M. Claeys, J.-J. Sinou, J.-P. Lambelin, R. Todeschini, Experimental and numerical study of the nonlinear vibrations of an assembly with friction joints, in: Proceedings of the 26th International Conference on Noise and Vibration engineering (ISMA2014), Leuven, Belgium, 2014.
[48] G. Kerschen, M. Peeters, J.-C. Golinval, A.F. Vakakis, Nonlinear normal modes, part i: A useful framework for the structural dynamicist, Mech. Syst. Signal Process. 23 (1) (2009) 170–194.
[49] M. Krack, L. Panning-von Scheidt, J. Wallaschek, A high-order harmonic balance method for systems with distinct states, J. Sound Vib. 332 (21) (2013) 5476–5488.
[50] T. Detroux, L. Renson, G. Kerschen, The harmonic balance method for advanced analysis and design of nonlinear mechanical systems, in: Proceedings of the 32th International Modal Analysis Conference (IMAC), Orlando, FL, USA, 2014.
[51] R.J. Kuether, M.R. Brake, M.S. Allen, Evaluating convergence of reduced order models using nonlinear normal modes, in: Model Validation and Uncertainty Quantification, vol. 3, Springer, 2014, pp. 287–300.
[52] D. Laxalde, F. Thouverez, Complex non-linear modal analysis for mechanical systems: Application to turbomachinery bladings with friction interfaces, J. Sound Vib. 322 (4) (2009) 1009–1025.
[53] M. Krack, L. Panning-von Scheidt, J. Wallaschek, C. Siewert, A. Hartung, Reduced order modeling based on complex nonlinear modal analysis and its application to bladed disks with shroud contact, J. Eng. Gas Turbines Power 135 (10) (2013) 102502.
[54] F. Schilder, H.M. Osinga, W. Vogt, Continuation of quasi-periodic invariant tori, SIAM J. Appl. Dyn. Syst. 4 (3) (2005) 459–488.
[55] L. Peletan, S. Baguet, M. Torkhani, G. Jacquet-Richardet, Quasi-periodic harmonic balance method for rubbing self-induced vibrations in rotor–stator dynamics, Nonlinear Dynam. 78 (4) (2014) 2501–2515.
[56] M. Guskov, F. Thouverez, Harmonic balance-based approach for quasi-periodic motions and stability analysis, J. Vib. Acoust. 134 (3) (2012) 031003.

[57] H. Liao, Global resonance optimization analysis of nonlinear mechanical systems: Application to the uncertainty quantification problems in rotor dynamics, Commun. Nonlinear Sci. Numer. Simul. 19 (9) (2014) 3323–3345.
[58] A. Grolet, F. Thouverez, Vibration of mechanical systems with geometric nonlinearities: Solving harmonic balance equations with groebner basis and continuations methods, in: Proceedings of the Colloquium Calcul des Structures et Modélisation CSMA, Giens, France, 2013.
[59] G.W. Hill, On the part of the motion of the lunar perigee which is a function of the mean motions of the sun and moon, Acta Math. 8 (1) (1886) 1–36.
[60] V. Lanza, M. Bonnin, M. Gilli, On the application of the describing function technique to the bifurcation analysis of nonlinear systems, IEEE Trans. Circuits Syst. Express Briefs II 54 (4) (2007) 343–347.
[61] F. Bonani, M. Gilli, Analysis of stability and bifurcations of limit cycles in chua's circuit through the harmonic-balance approach, IEEE Trans. Circuits Syst. I 46 (8) (1999) 881–890.
[62] F. Traversa, F. Bonani, S.D. Guerrieri, A frequency-domain approach to the analysis of stability and bifurcations in nonlinear systems described by differential-algebraic equations, Int. J. Circuit Theory Appl. 36 (4) (2008) 421–439.
[63] A. Lazarus, O. Thomas, A harmonic-based method for computing the stability of periodic solutions of dynamical systems, C. R. M. 338 (9) (2010) 510–517.
[64] F.L. Traversa, F. Bonani, Improved harmonic balance implementation of floquet analysis for nonlinear circuit simulation, AEU-Int. J. Electron. Commun. 66 (5) (2012) 357–363.
[65] C. Piccardi, Bifurcations of limit cycles in periodically forced nonlinear systems: The harmonic balance approach, IEEE Trans. Circuits Syst. I 41 (4) (1994) 315–320.
[66] C. Piccardi, Harmonic balance analysis of codimension-2 bifurcations in periodic systems, IEEE Transactions on Circuits and Systems – Part 1: Fundamental Theory and Applications 43 (1996) 1015–1018.
[67] M.J. Powell, A hybrid method for nonlinear equations, Numer. Methods Nonlinear Algebr. Equ. 7 (1970) 87–114.
[68] S. Nacivet, C. Pierre, F. Thouverez, L. Jezequel, A dynamic lagrangian frequency–time method for the vibration of dry-friction-damped systems, J. Sound Vib. 265 (1) (2003) 201–219.
[69] J.L. Hwang, T.N. Shiau, An application of the generalized polynomial expansion method to nonlinear rotor bearing systems, J. Vib. Acoust. 113 (3) (1991) 299–308.
[70] G. Xie, J.Y. Lou, Alternating frequency/coefficient (afc) technique in the trigonometric collocation method, Int. J. Non-Linear Mech. 31 (4) (1996) 531–545.
[71] S. Narayanan, P. Sekar, A frequency domain based numeric–analytical method for non-linear dynamical systems, J. Sound Vib. 211 (3) (1998) 409–424.
[72] C. Duan, R. Singh, Super-harmonics in a torsional system with dry friction path subject to harmonic excitation under a mean torque, J. Sound Vib. 285 (4) (2005) 803–834.
[73] T. Kim, T. Rook, R. Singh, Super-and sub-harmonic response calculations for a torsional system with clearance nonlinearity using the harmonic balance method, J. Sound Vib. 281 (3) (2005) 965–993.
[74] L. Peletan, S. Baguet, M. Torkhani, G. Jacquet-Richardet, A comparison of stability computational methods for periodic solution of nonlinear problems with application to rotordynamics, Nonlinear Dynam. 72 (3) (2013) 671–682.
[75] G. Moore, Floquet theory as a computational tool, SIAM J. Numer. Anal. 42 (6) (2005) 2522–2568.
[76] W. Govaerts, Y.A. Kuznetsov, V. De Witte, A. Dhooge, H. Meijer, W. Mestrom, A. Riet, B. Sautois, Matcont and cl Matcont: Continuation Toolboxes in Matlab, Tech. Rep, Gent University and Utrech University, 2011.
[77] R. Seydel, Practical Bifurcation and Stability Analysis, Springer, 2010.
[78] J. Guckenheimer, M. Myers, B. Sturmfels, Computing hopf bifurcations i, SIAM J. Numer. Anal. 34 (1) (1997) 1–21.
[79] W.-J. Beyn, A. Champneys, E. Doedel, W. Govaerts, Y.A. Kuznetsov, B. Sandstede, Numerical continuation, and computation of normal forms, in: Handbook of Dynamical Systems, vol. 2, 2002, pp. 149–219.
[80] N. Van Der Aa, H. Ter Morsche, R. Mattheij, Computation of eigenvalue and eigenvector derivatives for a general complex-valued eigensystem, Electron. J. Linear Algebra 16 (1) (2007) 300–314.
[81] J. Noël, L. Renson, G. Kerschen, Complex dynamics of a nonlinear aerospace structure: Experimental identification and modal interactions, J. Sound Vib. 333 (12) (2014) 2588–2607.
[82] L. Renson, J. Noël, G. Kerschen, Complex dynamics of a nonlinear aerospace structure: numerical continuation and normal modes, Nonlinear Dynam. 79 (2) (2015) 1293–1309.